IEEE Access
Multidisciplinary | Rapid Review | Open Access Journal

Received November 15, 2018, accepted December 18, 2018, date of publication December 25, 2018,
date of current version January 23, 2019.

Digital Object Identifier 10.1109/ACCESS.2018.2889702

Robust Cascade Path-Tracking Control of Networked Industrial Robot Using Constrained Iterative Feedback Tuning

YUANLONG XIE, JIAN JIN, XIAOQI TANG, BOSHENG YE, AND JIEYU TAO
School of Mechanical Science and Engineering, Huazhong University of Science and Technology, Wuhan 430074, China

Corresponding author: Jian Jin (jinjian1964@hust.edu.cn)

This work was supported in part by the National Science and Technology Major Project under Grant 2015ZX04002202 and in part by the National Natural Science Foundation of China under Grant 51675204, Grant 51475185, and Grant 61703376.

ABSTRACT Industrial robots can be found in many manufacturing applications that suffer from imprecise position control of their own drive systems due to unknown external disturbances and parametric uncertainties. To address this problem, this paper proposes a robust cascade path-tracking control method to achieve better position control performance for a networked industrial robot. In the joint task space, the cascade control framework is formulated for the developed robotic actuation system, which consists of an inner speed loop and an outer position loop. Instead of exploring the conventional model-based approaches, a multiple degree-of-freedom constrained iterative feedback tuning (CIFT) method is presented to regulate the cascade controller by utilizing the monitored process data straightforwardly. With the integration of the normalized input constraints and position tracking error, the proposed CIFT method seeks an optimal solution to track the desired position profiles with satisfactory accuracy and improved robustness. Theoretical analysis is performed to verify the asymptotical convergence of the closed-loop system. Implemented on a real-time networked industrial robot, experimental results demonstrate that the proposed method can enhance the dynamic path tracking and system robustness during various operating situations.

INDEX TERMS Cascade control, path-tracking, networked industrial robot, constrained iterative feedback tuning, input constraints.

I. INTRODUCTION

Nowadays, industrial robots are widely applied in the manufacturing fields, such as drilling, painting process, machining and part assembly, in where an industrial robot should be steered along a predefined position reference trajectory [1]–[3]. For this purpose, there exist extensive strategies concerned with the robotic path-tracking controller design, such as model predictive control [4], iterative learning control [5], sliding mode control [6] and their combinations [7], [8]. However, the precise path-tracking of an industrial robot is still challenging as the coupling characteristics among the actuators will generate complex mechanical dynamics. Moreover, the industrial robots have been toward electric-motor powered and servo-controlled directions. The dynamic tracking of the robotic actuation system is affected by the internal or external disturbances, system uncertainties and time-varying operating environment [9], [10]. Thereby, an improved path-tracking performance of an industrial robot is becoming necessary for the potential applications.

Among the existing positioning methods, cascade control method has the ability to attenuate the disturbances and enhance the system tracking simultaneously when single feedback control cannot achieve a satisfactory performance [11]. The cascade control systems are composed of two nested control loops, in where the output of the primary controller drives the inner secondary controller. Up to now, owing to the extra adjustable parameters and relatively simple implementation, some cascade control results tailored to the position path-following issues of the robotic systems have been reported. For instance, a cascade control algorithm is designed to separate the hydraulic dynamics of parallel robots from the mechanical part [12]; Nedic *et al.* [13] have developed a model-based cascade controller tuning method to provide precise control of the hydraulic actuator for a parallel robot platform; in the robotic joint space, a position motion controller is presented to make the actual hydraulic actuators conform to the desired reference [14]. The specific cascade structure of these robotic systems is beneficial to design

flexibilities and robust control. However, an explicit model of the robot to be controlled is required for implementation, which implies that additional information about the pose and the displacement of the end-effect should be obtained from direct kinematical estimations or multiple degree-of-freedom (DOF) sensors.

In practical physical systems, such as the robotic systems, it is still a tough task to get a priori knowledge of the high nonlinear and time-varying characteristics [15], [16]. As a result of that, the kinematical parameters or dynamical models of a robot are not easy to be identified [17], [18]. Modeling a plant is an approximation of the real system with unmodeled dynamics and parametric uncertainties, and therefore the resulting path-tracking errors of model-based methods cannot converge to a small attenuation level if the identified model is inaccurate. Moreover, recent studies have revealed inherent fractional-order features in the servo drive systems, which increases the difficulties to design a model-based cascade controller for such servo-controlled robots [19], [20]. Another underlying problem is that the existing cascade controllers are usually tuned sequentially via different techniques, i.e., the inner secondary controller is tuned first to give a faster tracking response, followed by the optimization of the outer primary controller [21]. In this context, as an industrial robot has multi-DOF actuators to be controlled, the consequential tuning complexities and consuming computation time cannot be neglected.

To overcome these limitations, iterative feedback tuning (IFT) strategy is considered for automatic tuning of the industrial robotic cascade system in this paper, which only relies on available input and output data measured from the experiments [22]. IFT can handle the nonlinear behaviors of the controlled plant with high precision and better insensitivity to external disturbances. The repetitive nature of the robot-executive manufacturing processes provides a good opportunity for IFT techniques. The recent years have witnessed IFT implemented in many industrial applications due to its superior model-free automatic tuning capacity [10], [23]–[26]. However, only a few IFT-involved researches target on the cascade system design: in [10], the IFT algorithm is adopted to tune a typical cascade speed and position control structure of a servo control system; in additional, adaptive controller for a real experimental quadcopter is proposed using cascade IFT method to adjust the vehicle angle [27]; data-driven IFT is used to tune the parameters of a cascade feedback controller minimizing an H_2 criterion as presented in [28]. On the other hand, communication networks have been employed for industrial processes and equipment to transmit the measurement output and control signal [29], [30]. Vast amounts of network data with sufficient information of the actual systems are generated and stored, which can be applied to directly design a controller [31]. Unlike the traditional point-to-point system, the network-controlled industrial robot guarantees a high-speed and reliable data transmission, which gives an opportunity to tune the cascade controllers using data-based IFT method.

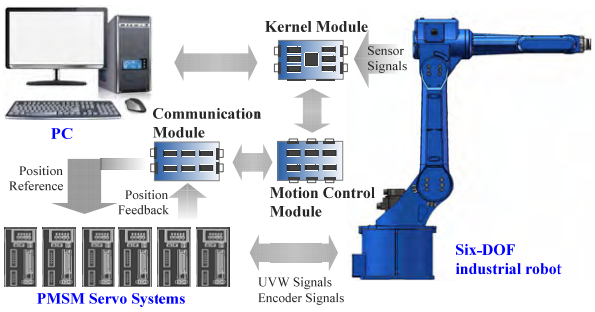

FIGURE 1. The developed networked industrial robot.

According to the authors' best knowledge, there are no explored works on the specific combinations of the IFT-based cascade system with multi-DOF industrial robots, which motivates us to integrate the IFT into robotic cascade system to improve its path-tracking performance.

For an industrial robot, the limited mechanical properties and saturation nonlinearities of actuation motors restrict its velocities, which is caused by the rate of the actuator inputs and the constraints of magnitude [32]. Higher overshoot, longer regulation time and deteriorative system stability may result from ignoring the input saturation effect. To design a robotic path-tracking controller, not only the following error should be eliminated, but also the control inputs should not exceed the bounds. For this purpose, there have been research works of the input-constrained tracking control for robotic systems, such as robot manipulators, mobile robot, and cable-suspended robot [33]–[37]. However, in the aforesaid robotic cascade control publications, it is implicitly assumed that the designed systems can furnish any required drive torque value, thus actuator saturations are typically omitted from the objective function to simplify the controller tuning. Beyond the saturation problem, in the industrial robot environments, the inherent robustness of the robotic systems is also alleviated by the external disturbances and parameter vibration. The resulting undesirable system behaviors or degraded closed-loop performance are inadequate to meet the practical precision requirements for an industrial robot.

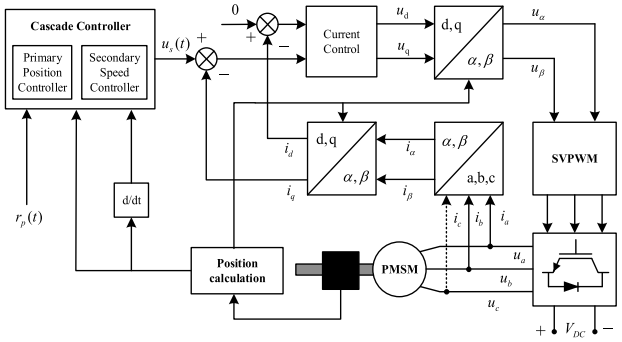

FIGURE 2. Field oriented control on an actuated joint.

Motivated by the above challenges, this paper proposes a practical constrained IFT (CIFT)-based cascade controller to

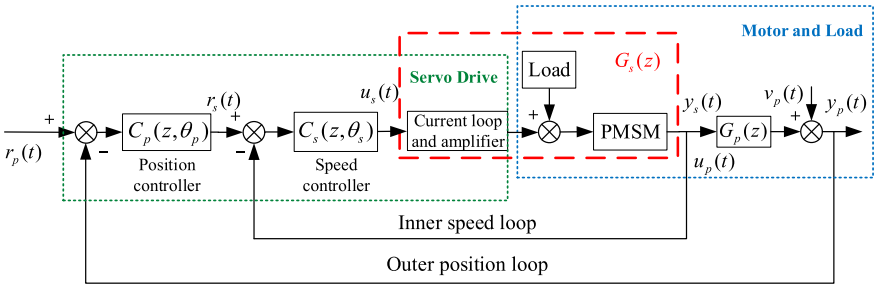

FIGURE 3. Block diagram of the proposed cascade position controller.

formulate a robust path-tracking of a networked industrial robot. Comparing with the existing ones, the distinguished features of the proposed method are threefold: (1) under unknown system dynamics, CIFT offers an effective way to utilize the monitored data requiring no explicit model information of the controlled industrial robot, which mitigates the shortcoming of the traditional model-based methods; (2) superior to the sequential tuning procedure, the proposed cascade controller, which can optimize the control parameters for the primary and secondary loops simultaneously, is easy to implement in the multi-DOF industrial robot due to its relatively lower computational burden; (3) to enhance the system robustness, input constraints are incorporated into the CIFT attaining a global optimum solution for the cascade controller, which has the capacity of mitigating the actuation saturation and achieving a satisfactory path-tracking performance.

The remainder of this paper is organized as follows. Section II describes the networked industrial robotic cascade control system. In Section III, a robust CIFT method is presented to optimize the cascade control parameters with consideration of the path-tracking error and normalized input constraints. Two illustrative experiments on a real-time networked industrial robot are conducted to verify the effectiveness of the developed robust cascade path-tracking method in Section IV. Finally, conclusions and future works are provided in Section V.

II. NETWORKED INDUSTRIAL ROBOTIC CASCADE CONTROL SYSTEM

A. NETWORKED INDUSTRIAL ROBOT

As illustrated in Fig. 1, a networked industrial robot is developed in this paper, the control architecture of which comprises a standard PC using the open-source Linux OS, an ARM cortex-A8 microprocessor interface, and permanent magnet synchronous motor (PMSM) servo control systems. Specifically, the upper PC provides the user interaction interface with functions of teaching simulations, numeric control, signal animation and debugging, etc; the microprocessor controller, consisting of a kernel module, a motion control module and a communication module, is mainly responsible for decoding position, interpolation, path planning, position reference transmitting for each servo drive while it receives the current position; PMSM servo systems are used to drive each joint so that the developed industrial robot can realize the desired movement of the end-effector. To satisfy the real-time requirements, industrial network, often referred as fieldbus, is applied for the developed industrial robotic servo control systems due to its remarkable advantages of reduction of wiring, ease of maintenance, remote operation and reliable data transmission [35]. The developed communication network protocol here is EtherCAT protocol with 1 *ms* cycle time. The network technology meets the requirements of multi-axis, multi-channel, short communication period of an industrial robot. To guarantee the practicability and reliability for data-transmission, the developed EtherCAT processes the following network technical characteristics and mechanisms: bicyclic redundant hardware architecture, data packet retransmission, error detection and handling.

Remark 1: In In this paper, the EtherCAT network is employed for the process data communication, including the control input signal, position command/feedback, and control parameters. For the networked industrial system, lots of data can be received and stored at each communication cycle. Model-based control theories are only available when accurate mathematic models can be identified by historical or real-time data. In comparison, the direct utilization of these data for controller design and theoretical analysis is efficient and meaningful. Hence, we focus on the cascade position-following controller design based on the data-driven model-free IFT method using the network-transmitted input/output data.

B. CASCADE POSITION CONTROLLER

In practice, the efficiency and tracking performance of an industrial robot mainly depend on the dynamic response of its own drive systems. In the joint space coordinate, a cascade field oriented control framework is employed for the mechatronic joints actuated by the PMSM as shown in Fig. 2, and a primary position controller and a secondary speed controller are designed to achieve a satisfactory path-tracking for the developed robot. The simplified block diagram of the robotic cascade path-tracking control system is presented in Fig. 3. As shown in Fig. 3, the inner speed loop consists of a speed controller $C_s(z, \theta_s)$ parameterized by θ_s and the loop model $G_s(z)$ while the outer position loop includes a position controller $C_p(z, \theta_p)$ parameterized by θ_p and the position loop model $G_p(z)$. Define $u_s(t)$ and $u_p(t)$ as the control inputs of the

inner speed loop and outer position loop, respectively. Then, the discrete-time cascade process can be described as follows

$$y_s(t) = G_s(z)u_s(t) \tag{1}$$
$$y_p(t) = G_p(z)u_p(t) + v_p(t) \tag{2}$$

where $y_s(t)$ and $y_P(t)$ are the output signals of the inner speed loop and outer position loop, respectively, and $v_p(t)$ are the measurement noises and disturbances. For the cascade control process, the output from the inner process becomes the input to the outer process, i.e., $u_p(t) = y_s(t)$.

Furthermore, substituting the reference signal $r_p(t)$ into (1) and (2), the cascade robotic system is reformulated as

$$y_p(t, \theta_s, \theta_p) = T_p(z, \theta_s, \theta_p)r_p(t) + S_p(z, \theta_s, \theta_p)v_p(t) \tag{3}$$
$$y_s(t, \theta_s, \theta_p) = T_s(z, \theta_s, \theta_p)(r_p(t) - v_p(t)) \tag{4}$$
$$\begin{aligned} u_s(t) &= \frac{T_s(z, \theta_s, \theta_p)}{G_s}(r_p(t) - v_p(t)) \\ &= \frac{T_p(z, \theta_s, \theta_p)}{G_sG_p}(r_p(t) - v_p(t)) \end{aligned} \tag{5}$$

where

$$T_i(z, \theta_s) = \frac{C_s(z, \theta_s)G_s(z)}{1 + C_s(z, \theta_s)G_s(z)} \tag{6}$$
$$T_p(z, \theta_s, \theta_p) = \frac{C_p(z, \theta_p)T_i(z, \theta_s)G_p(z)}{1 + C_p(z, \theta_p)T_i(z, \theta_s)G_p(z)} \tag{7}$$
$$T_s(z, \theta_s, \theta_p) = \frac{T_p(z, \theta_s, \theta_p)}{G_p(z)} \tag{8}$$
$$S_p(z, \theta_s, \theta_p) = 1 - T_p(z, \theta_s, \theta_p) \tag{9}$$

To ensure potential control performance of the developed cascade controller, the crucial task is the tuning of its control parameters contributing to design flexibility and control superiority. This paper explores a model-free tuning solution for the cascade controller so that the closed-loop system can achieve a precise path-tracking, despite the modeling uncertainties and unknown system dynamics.

III. MULTI-DOF CASCADE POSITION CONTROLLER TUNING

In the manufacturing applications, the joint typically perform tasks in a specific repetitive manner. Given this context, this paper proposes an iteration-related optimization method for the cascade position controller, as demonstrated by the following results.

A. CASCADE ITERATIVE FEEDBACK TUNING

To guarantee that the PMSM servo drive tracks the desired trajectory $y_d(t)$ for each joint, we consider the following objective $J(\theta_s, \theta_p)$ with respect to the tracking error and controller input magnitude

$$J(\theta_s, \theta_p) = \frac{1}{2N}\left[\sum_{t=1}^{N}(y_p(t, \theta_s, \theta_p) - y_d(t))^2 + \lambda\sum_{t=1}^{N}u_s(t, \theta_s, \theta_p)^2\right] \tag{10}$$

where λ denotes a pre-defined weighting factor.

By defining $\boldsymbol{\theta} = [\theta_s\ \theta_p]^{\mathrm{T}}$, the optimal cascade control parameters vector $\boldsymbol{\theta}^*$ can be derived as

$$\boldsymbol{\theta}^* = \arg\min_{\boldsymbol{\theta}} J(\boldsymbol{\theta}) \tag{11}$$

Considering that the gradient of (10) depends on the partial derivative of y_p and u_s in relation to θ_s and θ_p, we have

$$\frac{\partial J(\boldsymbol{\theta})}{\partial(\boldsymbol{\theta})} = \frac{1}{N}\left[\sum_{t=1}^{N}(y_p(t, \boldsymbol{\theta}) - y_d(t))\frac{\partial y_p(t, \boldsymbol{\theta})}{\partial(\boldsymbol{\theta})} + \lambda\sum_{t=1}^{N}u_s(t)\frac{\partial u_s(t)}{\partial(\boldsymbol{\theta})}\right] \tag{12}$$

Dropping the dependence on $\boldsymbol{\theta}$ for simplification reason yields

$$\begin{aligned} \frac{\partial J(\boldsymbol{\theta})}{\partial \boldsymbol{\theta}} &= \left[\frac{\partial J(\boldsymbol{\theta})}{\partial \theta_s}\ \frac{\partial J(\boldsymbol{\theta})}{\partial \theta_p}\right]^{\mathrm{T}} \\ &= \begin{bmatrix} \frac{1}{N}\sum_{t=1}^{N}\left((y_p(t) - y_d(t))\frac{\partial y_p(t)}{\partial \theta_s} + \lambda u_s(t)\frac{\partial u_s(t)}{\partial \theta_s}\right) \\ \frac{1}{N}\sum_{t=1}^{N}\left((y_p(t) - y_d(t))\frac{\partial y_p(t)}{\partial \theta_p} + \lambda u_s(t)\frac{\partial u_s(t)}{\partial \theta_p}\right) \end{bmatrix} \end{aligned} \tag{13}$$

According to (7), it can be obtained that

$$\begin{aligned} \frac{\partial T_p}{\partial \theta_s} &= \frac{\partial}{\partial \theta_s}\left(\frac{C_pT_iG_p}{1 + C_pT_iG_p}\right) \\ &= \frac{\partial C_s}{\partial \theta_s}\left[\frac{C_pG_p}{(1 + C_pT_iG_p)^2}\frac{G_s}{(1 + C_sG_s)^2}\right] \end{aligned} \tag{14}$$
$$\begin{aligned} \frac{\partial T_p}{\partial \theta_p} &= \frac{\partial}{\partial \theta_p}\left(\frac{C_pT_iG_p}{1 + C_pT_iG_p}\right) \\ &= \frac{\partial C_p}{\partial \theta_p}\left[\frac{T_iG_p}{(1 + C_pT_iG_p)^2}\right] \end{aligned} \tag{15}$$

The combination of (3)-(5), (14) and (15) gives the partial derivative of y_p with respect to θ_s and θ_p

$$\begin{aligned} \frac{\partial y_p}{\partial \theta_s} &= \frac{\partial}{\partial \theta_s}(T_pr_p + S_pv_p) = \frac{\partial}{\partial \theta_s}(T_pr_p - T_pv_p + v_p) \\ &= \frac{\partial C_s}{C_s\partial \theta_s}\left[\frac{C_pG_p}{(1 + C_pT_iG_p)^2}\frac{C_sG_s}{(1 + C_sG_s)^2}(r_p - v_p)\right] \\ &= \frac{\partial C_s}{C_s\partial \theta_s}\left[T_p(r_p - y_p) - \frac{T_s}{C_p}(y_p - v_p)\right] \\ \frac{\partial y_p}{\partial \theta_p} &= \frac{\partial}{\partial \theta_p}(T_pr_p - T_pv_p + v_p) \\ &= \frac{\partial C_p}{\partial \theta_p}\left[\frac{T_iG_p}{(1 + C_pT_iG_p)^2}(r_p - v_p)\right] \\ &= \frac{\partial C_p}{C_p\partial \theta_p}\left[\frac{C_pT_iG_p}{(1 + C_pT_iG_p)^2}r_p - \frac{C_pT_iG_p}{(1 + C_pT_iG_p)^2}v_p\right] \\ &= \frac{\partial C_p}{C_p\partial \theta_p}\left[T_p(r_p - y_p)\right] \end{aligned} \tag{16}$$
$$\tag{17}$$

Similar to the above analysis, the partial derivatives of u_s in regards to θ_s and θ_p are derived as

$$\begin{aligned}\frac{\partial u_s}{\partial \theta_s} &= \frac{\partial}{\partial \theta_s}\left[\frac{T_p}{G_sG_p}(r_p - v_p)\right] \\ &= \frac{\partial C_s}{C_s\partial\theta_s}\left[\frac{C_pG_p}{G_sG_p(1+C_pT_iG_p)^2}\frac{C_sG_s}{(1+C_sG_s)^2}(r_p - v_p)\right] \\ &= \frac{\partial C_s}{C_s\partial\theta_s}\left[\frac{T_p}{G_sG_p}(r_p - y_p) - \frac{T_s}{G_sG_pC_p}(y_p - v_p)\right] \\ &= \frac{\partial C_s}{C_s\partial\theta_s}\left[\frac{T_p}{G_sG_p}(r_p - y_p) - \frac{T_p}{G_pG_sG_pC_p}(y_p - v_p)\right] \\ \frac{\partial u_s}{\partial \theta_p} &= \frac{\partial}{\partial \theta_p}\left[\frac{T_p}{G_sG_p}(r_p - v_p)\right] \qquad (18) \\ &= \frac{\partial C_p}{C_p\partial\theta_p}\left[\frac{C_pT_iG_p}{G_sG_p(1+C_pT_iG_p)^2}(r_p - v_p)\right] \\ &= \frac{\partial C_p}{C_p\partial\theta_p}\left[\frac{T_p}{G_sG_p}(r_p - y_p)\right] \qquad (19)\end{aligned}$$

Therefore, the descent-gradient of the objective function considering the nested cascade control parameters is determined by

$$\frac{\partial y_p}{\partial \boldsymbol{\theta}} = \begin{bmatrix}\frac{\partial y_p}{\partial \theta_s} \\ \frac{\partial y_p}{\partial \theta_p}\end{bmatrix} = \begin{bmatrix}\frac{\partial C_s}{C_s\partial\theta_s}\left[T_p(r_p - y_p) - \frac{T_s}{C_p}(y_p - v_p)\right] \\ \frac{\partial C_p}{C_p\partial\theta_p}\left[T_p(r_p - y_p)\right]\end{bmatrix} \qquad (20)$$

$$\begin{aligned}\frac{\partial u_s}{\partial \boldsymbol{\theta}} &= \begin{bmatrix}\frac{\partial u_s}{\partial \theta_s} & \frac{\partial u_s}{\partial \theta_p}\end{bmatrix}^{\mathrm{T}} \\ &= \begin{bmatrix}\frac{\partial C_s}{C_s\partial\theta_s}\left[\frac{T_p(r_p - y_p)}{G_sG_p} - \frac{T_p(y_p - v_p)}{G_pG_sG_pC_p}\right] \\ \frac{\partial C_p}{C_p\partial\theta_p}\left[\frac{T_p}{G_sG_p}(r_p - y_p)\right]\end{bmatrix} \qquad (21)\end{aligned}$$

In this paper, the system model G_s is assumed to be unknown, one reason lies in its general form containing time-varying control coefficients, unclear parameters and unpredictable uncertainties. As for G_p, since it typically indicates the relationship between the speed feedback and position feedback, it can be derived directly, i.e., it is $1/s$ in the developed networked industrial robot. As shown in (20) and (21), the gradients of the objective function cannot be obtained when the system model G_s is identified inaccurately. To solve this problem, inspired by the conventional IFT idea, three iterative experiments are performed so that the corresponding received data can be applied to estimate (20) and (21) as follows:

➢ First experiment: $r_p^1 = r^1$

$$y_p^1 = T_pr^1 + S_pv_p^1,\ \ y_s^1 = T_sr^1 - T_sv_p^1,\ \ u_s^1 = \frac{T_pr^1 - T_pv_p^1}{G_sG_p} \qquad (22)$$

➢ Second experiment: $r_p^2 = r^1 - y_p^1$

$$y_p^2 = T_p(r^1 - y_p^1) + S_pv_p^2,\ \ y_s^2 = T_s(r^1 - y_p^1) - T_sv_p^2,\ \ u_s^2 = \frac{T_p(r^1 - y_p^1) - T_pv_p^2}{G_sG_p} \qquad (23)$$

➢ Third experiment: $r_p^3 = r^1$

$$y_p^3 = T_pr^1 + S_pv_p^3,\ \ y_s^3 = T_sr^1 - T_sv_p^3,\ \ u_s^3 = \frac{T_pr^1 - T_pv_p^3}{G_sG_p} \qquad (24)$$

Then, the following estimators are constructed for the partial derivatives of y_p and u_s in (20) and (21)

$$\widehat{\frac{\partial y_p}{\partial \boldsymbol{\theta}}} = \begin{bmatrix}\widehat{\frac{\partial y_p}{\partial \theta_s}} & \widehat{\frac{\partial y_p}{\partial \theta_p}}\end{bmatrix}^{\mathrm{T}} = \begin{bmatrix}\frac{\partial C_s}{C_s\partial\theta_s}\left(y_p^2 - \frac{y_s^3 - y_s^2}{C_p}\right) \\ \frac{\partial C_p}{C_p\partial\theta_p}\left(y_p^2\right)\end{bmatrix} \qquad (25)$$

$$\widehat{\frac{\partial u_s}{\partial \boldsymbol{\theta}}} = \begin{bmatrix}\widehat{\frac{\partial u_s}{\partial \theta_s}} & \widehat{\frac{\partial u_s}{\partial \theta_p}}\end{bmatrix}^{\mathrm{T}} = \begin{bmatrix}\frac{\partial C_s}{C_s\partial\theta_s}\left(u_s^2 - \frac{u_s^3 - u_s^2}{G_pC_p}\right) \\ \frac{\partial C_p}{C_p\partial\theta_p}\left(u_s^2\right)\end{bmatrix} \qquad (26)$$

The estimation of the objective function (12) is finally achieved by

$$\widehat{\frac{\partial J(\boldsymbol{\theta})}{\partial \boldsymbol{\theta}}} = \frac{1}{N}\sum_{t=1}^{N}\left[\left(y_p^1 - y_d\right)\widehat{\frac{\partial y_p}{\partial \boldsymbol{\theta}}} + \lambda u_s^1\widehat{\frac{\partial u_s}{\partial \boldsymbol{\theta}}}\right] \qquad (27)$$

Here, the components $\left(y_p^1 - y_d\right)$ and u_s^1 contains the noise from the first experiment while the estimations of $\left(\partial y_p/\partial \boldsymbol{\theta}\right)$ and$(\partial u_s/\partial \boldsymbol{\theta})$ are computed using data from different experiments. It is reasonably assumed that v_p is mutually independent bounded stochastic noise of the system, and r_p is quasi-stationary and uncorrelated with the noises. Hence, the unbiased estimation of the objective gradient can be obtained.

The minimization of the objective function is realized by iterative updating law of the cascade position controller

$$\boldsymbol{\theta}_j^{i+1} = \boldsymbol{\theta}_j^i - \gamma_j^i\left(R_j^i\right)^{-1}\widehat{\frac{\partial J(\boldsymbol{\theta}_j^i)}{\partial \boldsymbol{\theta}_j}} \qquad (28)$$

where j denotes j-th actuated joint, i denotes the iteration, γ_j^i is the positive step size and R_j^i is determined by the following Gauss-Newton approximation of the Hessian matrix to speed up the convergence

$$\begin{aligned}R_j^i = \frac{1}{N}\sum_{t=1}^{N}\Bigg\{&\left[\widehat{\frac{\partial y_{p,j}}{\partial \boldsymbol{\theta}_j}}(\boldsymbol{\theta}_j^i)\right]\left[\widehat{\frac{\partial y_{p,j}}{\partial \boldsymbol{\theta}_j}}(\boldsymbol{\theta}_j^i)\right]^{\mathrm{T}} \\ &+\lambda\left[\widehat{\frac{\partial u_{s,j}}{\partial \boldsymbol{\theta}_j}}(\boldsymbol{\theta}_j^i)\right]\left[\widehat{\frac{\partial u_{s,j}}{\partial \boldsymbol{\theta}_j}}(\boldsymbol{\theta}_j^i)\right]^{\mathrm{T}}\Bigg\} \qquad (29)\end{aligned}$$

Remark 2: For (28), R_j^i is a positive definite matrix determining the descent-gradient direction, and the positive step size γ_j^i serves as the learning gain controlling the rate of the change between the parameters of the new controller and the previous one. Note that the step size plays a dominant role in maintaining the convergence and stability of the optimization. To be more specific, a large step size will lead to faster convergence properties while achieving better stability.

Thereby, as studied in [38], the step size should be chosen to satisfy that: (1) the resulting system converges to a local minimum of the cost function; (2) the stability of the closed-loop system is ensured. In association with the theoretical analysis in the next section, the step size is selected as $0 < \gamma_j^i = \{a_1, a_2\}/N \leq 1$ to guarantee a stable closed-loop system, where $0 < a_1 < a_2$ are pre-defined coefficients to obtain a stable and converged closed-loop system. In this way, faster tuning convergence and improved stability can be guaranteed during the tuning process.

B. CONTROL INPUT CONSTRAINTS

To address the actuator torque saturation phenomenon and enhance the system robustness, the following traditional anti-windup function is introduced to limit the control input magnitude

$$u(u_s) = sat(u_s) = \begin{cases} u_{\max} & \text{if } u_s \geq u_{\max} \\ u_s & \text{if } u_{\min} < u_s < u_{\max} \\ u_{\min} & \text{if } u_s \leq u_{\min} \end{cases} \tag{30}$$

where u_s denotes the input signal generated by the cascade controller, $u_{\min}$ and $u_{\max}$ are the minimum and maximum control inputs, respectively.

Inspired by Wang *et al.* [39], this paper presents the following function to provide a smooth approximation for $u(u_s)$ to further tackle the input saturation

$$h(u_s) = \begin{cases} u_{\max} \tanh\left(\dfrac{u_s}{u_{\max}}\right) \\ \quad = u_{\max} \dfrac{e^{u_s/u_{\max}} - e^{-u_s/u_{\max}}}{e^{u_s/u_{\max}} + e^{-u_s/u_{\max}}}, & u_s \geq 0 \\ u_{\min} \tanh\left(\dfrac{u_s}{u_{\min}}\right) \\ \quad = u_{\min} \dfrac{e^{u_s/u_{\min}} - e^{-u_s/u_{\min}}}{e^{u_s/u_{\min}} + e^{-u_s/u_{\min}}}, & u_s < 0 \end{cases} \tag{31}$$

By employing (31), the saturation function can be described as

$$u(u_s) = h(u_s) + \Delta(u_s) \tag{32}$$

where $\Delta(u_s) = sat(u_s) - h(u_s)$ is the difference between $sat(u_s)$ and $h(u_s)$, which is a bounded function satisfying the following inequality

$$\begin{aligned} |\Delta(u_s)| &= |sat(u_s) - h(u_s)| \leq u' \\ u' &= \max\left\{u_{\max}\left(1 - \tanh(1)\right), u_{\min}\left(\tanh(1) - 1\right)\right\} \end{aligned} \tag{33}$$

According to (33), $\Delta(u_s)$ will converge to 0 when the control input signal reaches the limitations. In contrast, $\Delta(u_s)$ approaches upper/lower limit from 0 if $|u_s|$ is located in the limited range $[u_{\min}, u_{\max}]$. As shown in Fig. 4, the proposed saturation function $h(u_s)$ is capable of improving the system dynamic smoothly.

To enhance the system robustness, as shown in (10), the performance criterion is subject to input constraints, which complicate the cascade controller design together with

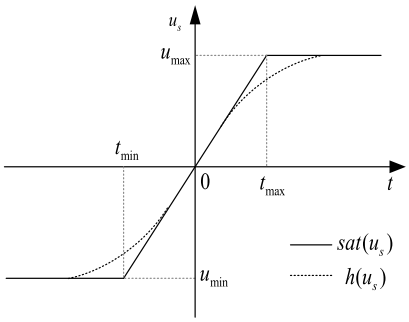

FIGURE 4. The comparison of the control input limitation functions.

the path-tracking error. In other words, a suitable trade-off between the primary tracking performance and the constraining on the control input is imposed on the objective function. In practice, a prior control goal must be accomplished to guarantee satisfactory system behaviors. An additional consideration can be further integrated into the criterion, which improves the comprehensive performance of the closed-loop system. The weighting factor may vary greatly as the potential systems being controlled have diverse requirements for the control input. In this paper, the tracking criterion has priority over the input signal limitation. Considering that, an optimal adjustment should be conducted for the weighting factor and thus a normalizing coefficient K_n is presented to achieve a balance between the path-tracking error and control input constraints

$$K_n = \frac{y_{\max} - y_{\min}}{u_{\max} - u_{\min}} \tag{34}$$

where $y_{\max}$ and $y_{\min}$ are the maximum and minimum value of the desired position, respectively.

Substituting the normalizing coefficient K_n into the designed objective function results in

$$J_n(\rho) = \min_{\rho} \left\{ \frac{1}{2N} \sum_{t=1}^{N} \left[y_p - y_d\right]^2 + \lambda K_n \frac{1}{2N} \sum_{t=1}^{N} (u_s)^2 \right\} \tag{35}$$

With the normalized design criterion (35), it becomes possible to make the trade-off of the CIFT method suitable for various applications. As the developed networked industrial robot has multiple joints need to be controlled, the final global solution with the normalized design criterion is given by

$$\begin{aligned} \boldsymbol{\theta}_j^{i+1} &= \boldsymbol{\theta}_j^i - \gamma_j^i \left(R_{n,j}^i\right)^{-1} \left[\widehat{\frac{\partial J_n}{\partial \boldsymbol{\theta}_j}}(\boldsymbol{\theta}_j^i)\right] \\ \widehat{\frac{\partial J_n}{\partial \theta}}(\theta_j^i) &= \frac{1}{N} \sum_{t=1}^{N} \left(\widehat{\frac{\partial y_{p,j}}{\partial \theta}} \left(y_{p,j}^1 - y_d\right) + \lambda K_{n,j} u_{s,j}^1 \widehat{\frac{\partial u_{s,j}}{\partial \theta}} \right) \\ R_{n,j}^i &= \frac{1}{N} \sum_{t=1}^{N} \left\{ \left[\widehat{\frac{\partial y_{p,j}}{\partial \boldsymbol{\theta}_j}}(\boldsymbol{\theta}_j^i)\right] \left[\widehat{\frac{\partial y_{p,j}}{\partial \boldsymbol{\theta}_j}}(\boldsymbol{\theta}_j^i)\right]^{\mathrm{T}} \right. \\ &\quad \left. + \lambda K_{n,j} \left[\widehat{\frac{\partial u_{s,j}}{\partial \boldsymbol{\theta}_j}}(\boldsymbol{\theta}_j^i)\right] \left[\widehat{\frac{\partial u_{s,j}}{\partial \boldsymbol{\theta}_j}}(\boldsymbol{\theta}_j^i)\right]^{\mathrm{T}} \right\} \end{aligned} \tag{36}$$

Remark 3: Here, the essential differences between the proposed method and the existing ones are emphasized as: 1) different with the traditional model-based methods depending on system identification accuracy, data-driven tuning mechanism is presented to regulate the control parameters in the absence of system explicit parametric models; 2) unlike conventional cascade control strategies, this method can tune the nested control loops concurrently to guarantee the optimization efficiency as the calculation burdens and the complexities of data processing are reduced significantly; 3) the normalized input constraints, which is usually omitted in the existing criterions, are consolidated into the objective function to alleviate the actuator saturation and achieve a robust path-tracking.

To summarize, the following concludes the procedure of the CIFT method:

1) Determine the initial control parameters for the developed algorithm;
2) Perform three iterative experiments based on (22)-(23);
3) Calculate the partial derivatives via (25) and (26);
4) Optimize the optimal parameters according to (36);
5) If the stop condition is satisfied, finish the tuning; otherwise, set $i = i + 1$ and go back to 2) for the next iteration cycle.

C. THEORETICAL ANALYSIS

The theoretical analysis of this paper is divided into two parts: the former establishes the convergence of the closed-loop system while the other part verifies the asymptotic accuracy of the tuning procedure.

Part 1 (The Tuning Convergence): As studied in the traditional IFT method [38], the asymptotical convergence of the CIFT can be guaranteed if it is implemented with an unbiased gradient estimation of the objective criterion and a convergent step size.

This paper performs three specific experiments to obtain the necessary data for the descent gradient calculation, which can be implemented without identifying a dynamic model of the system to be controlled. From (22) to (26), we have

$$\widehat{\frac{\partial y_p}{\partial \boldsymbol{\theta}}} = \frac{\partial y_p}{\partial \boldsymbol{\theta}} + \begin{bmatrix} \dfrac{\partial C_s}{C_s \partial \theta_s}\left(S_p v_p^2 - \dfrac{T_s v_p^1 + T_s v_p^2 - T_s v_p^3}{C_p}\right) \\ \dfrac{\partial C_p}{C_p \partial \theta_p}\left(S_p v_p^2\right) \end{bmatrix} \tag{37}$$

$$\widehat{\frac{\partial u_s}{\partial \boldsymbol{\theta}}} = \frac{\partial u_s}{\partial \boldsymbol{\theta}} + \frac{T_p}{G_s G_p}\begin{bmatrix} \dfrac{\partial C_s}{C_s \partial \theta_s}\left(-v_p^2 - \dfrac{v_p^1 + v_p^2 - v_p^3}{G_p C_p}\right) \\ \dfrac{\partial C_p}{C_p \partial \theta_p}\left(-v_p^2\right) \end{bmatrix} \tag{38}$$

Note that v_p^1, v_p^2 and v_p^3 are mutually independent bounded under the assumption that the experiments are sufficiently separated in time-domain, so that the gradient estimation of the objective function turns out to be unbiased. Moreover, the configuration of $0 < \gamma_j^i \leq 1$ meet the requirements of a suitable step size since

$$\sum_{i=1}^{\infty} \gamma_j^i = \infty, \quad \sum_{i=1}^{\infty} \left[\gamma_j^i\right]^2 < \infty \tag{39}$$

Therefore, the final tuned cascade controller approaches an optimum solution with guaranteed convergence.

Part II: (Asymptotic Accuracy Of The Proposed Method): According to the gradient calculation variability, we are now to quantify the asymptotic accuracy of the proposed CIFT method. As the proposed method tends toward the gradient-based descent direction, it is concluded that the optimization error is an asymptotical distribution with zero mean and covariance matrix $\sum$, i.e.,

$$\begin{aligned} &\sqrt{N}(\boldsymbol{\theta}_j^i - \tilde{\boldsymbol{\theta}}_j) \xrightarrow{D} N(0, \Sigma) \\ &\sum = a^2 \int_0^{\infty} e^{(C^j)t} \left(R_j\right)^{-1} \mathrm{Cov}\left[\frac{\partial J_n}{\partial \boldsymbol{\theta}}(\tilde{\boldsymbol{\theta}}_j)\right] \left(R^j\right)^{-1} e^{(C^j)^{\mathrm{T}} t} dt \\ &C^j = (1/2)I - a\left(R_{n,j}^i\right)^{-1} H_j(\tilde{\boldsymbol{\theta}}_j) \end{aligned} \tag{40}$$

where the constant R_j and $\tilde{\boldsymbol{\theta}}_j$ denote the stabilized $R_{n,j}^i$ and $\boldsymbol{\theta}_j^i$, respectively, $H_j(\tilde{\boldsymbol{\theta}}_j)$ denotes the Hessian Matrix of $J_N(\boldsymbol{\theta}_j^i)$ when $\boldsymbol{\theta}_j^i = \tilde{\boldsymbol{\theta}}_j$, $a = \gamma_j^i N$, I is the unit diagonal matrix. The proof of the above-mentioned results is very similar to the gradient estimated control systems [40], which can be extended to this paper and it is therefore omitted here.

Remark 4: The above-mentioned results quantify the asymptotic accuracy of the developed CIFT-tuned cascade controller, which crucially depends on the covariance of the descent-gradient computation. Furthermore, as presented in [41], an optimal prefilter can be constructed to enhance the accuracy of the IFT, which leads to a relatively small covariance matrix. However, the output of the plant under normal operating conditions, i.e., with zero reference signal, is required to collect large amounts of data to compute the optimal prefilter. Considering the tuning efficiency and calculation burden, the contribution of the optimal prefilter is considered as being negligible in the practical robotic application in this paper.

IV. EXPERIMENTAL VERIFICATION

A. EXPERIMENTAL SETUP

To carried out the experiments, a six-DOF networked industrial robot actuated by the PMSMs is considered, as shown in Fig. 5. The overall implementation architecture consists of three layers: (1) the terminal conversation layer realizes the human-machine interaction so that the users can customize their own instructions through teaching program; (2) the decision layer completes the multi-axis interpolation and the proposed cascade path-tracking controller tuning; (3) the behavior layer provides the drivers for the actuator devices, including PMSM servo systems and I/O devices, and the end-effect of the industrial robot can achieve the reference position. EtherCAT industrial network is served as the communication interface between the decision layer and

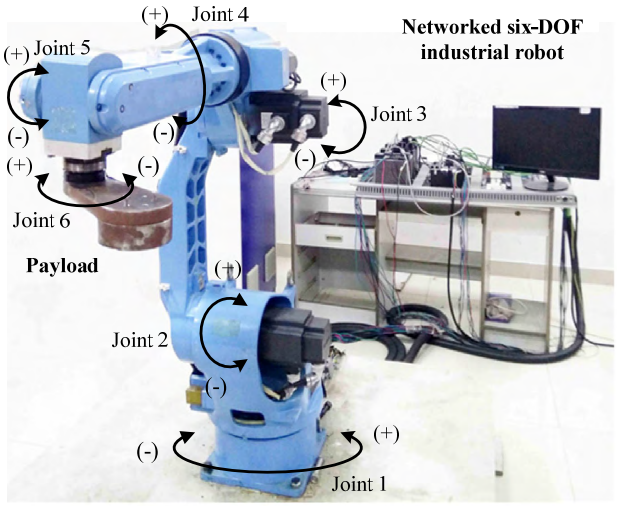

FIGURE 5. Six-DOF networked industrial robot.

TABLE 1. Specifications of the networked industrial robot.

Parameters	Joint					
	1	2	3	4	5	6
Range (°)	±170	+75 −170	+45 −265	±180	±108	±360
Rated speed (rad/s)	2.58	2.58	2.58	6.28	3.93	6.28

the behaviors layer. For the developed robotic drive system, the powertrain of each actuated joint is composed of a servo motor, a reducer and external load. The specifications of the networked industrial robot are provided by Table 1.

The joints actuated by PMSM are controlled individually using a cascade controller with the optimal control parameters regulated using the implemented CIFT algorithm, as demonstrated in Fig 6. Through inverse kinematics, the reference and feedback position of each joint are evaluated from the desired orientation ρ'_{XYZ} and the feedback end-effector orientation ρ_{XYZ}, separately. For the developed networked robotic cascade system, we typically employ the proportional controller $\theta_p = [K_p]$ and the proportional-integral controller $\theta_s = [K_s \ K_I]^{\mathrm{T}}$ for the inner speed loop and the outer position loop, respectively, which implies

$$C_s = K_s + K_I \frac{T^2 z^2}{Tz^2 - Tz} = \left[\frac{Tz^2 - Tz}{Tz^2 - Tz} \ \frac{T^2 z^2}{Tz^2 - Tz} \right] \theta_s \tag{41}$$

$$C_p = K_p = \theta_p \tag{42}$$

where $T = 1\ ms$ denotes the sampling time.

To implement the proposed CIFT method, the step size for K_p, K_s and K_I are specified as 0.01, 0.0001, 0.01, respectively, and λ is set as 0.001. The baseline control parameters $\theta_p = [0.78]$, $\theta_s = [2.34, 0.0200]$ sequentially tuned by trail and error are used for benchmarking and comparison purpose, and it can help in converging to the optimal solution sooner.

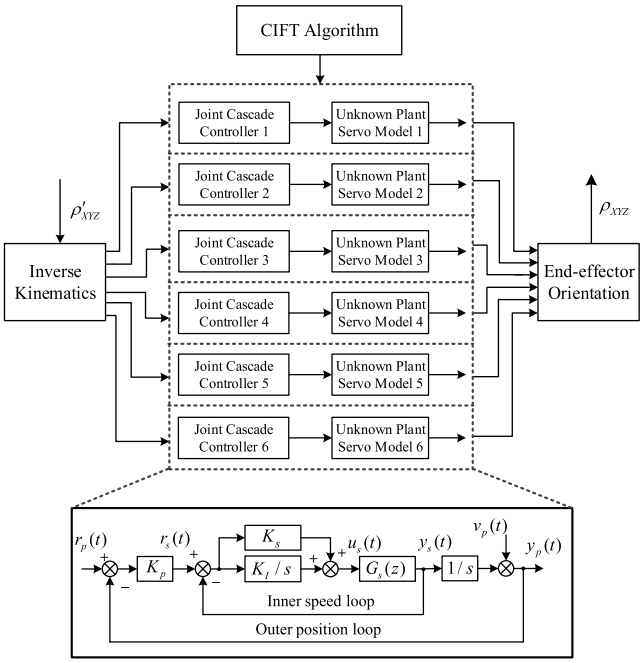

FIGURE 6. The implementation of the cascade path-tracking controller.

B. EXPERIMENTAL RESULTS

To verify the feasibility and reliability of the proposed CIFT-tuned cascade controller, we consider a typical repetitive reference for the palletizing application using a desired profile with a period of 6 s. An additional 5.32 kg payload can be added to the end-effect so that more time-varying external disturbances are provided to verify the robustness of the proposed cascade controller. For the comparative experiments, two cases of without (Case 1) or with (Case 2) payload are studied to demonstrate the effectiveness and applicability of the developed robust cascade path-tracking control method.

TABLE 2. The tuned parameters using CIFT method in Case 1.

Parameters	Joint					
	1	2	3	4	5	6
K_p	1.10	1.32	1.13	0.78	1.33	0.80
K_s	3.97	3.56	3.85	2.74	4.17	2.78
K_I	0.0253	0.0267	0.0298	0.0201	0.0431	0.0202

1) *Case 1:* For the palletizing application, the position references of joint 4 and 6 remain zero during the normal operation. The converged control parameters are given in Table 2. The position responses and tracking errors of PMSM-actuated joints are shown in Fig. 7 and Fig. 8, respectively. As shown in Fig. 8, the traditional model-based cascade controller is not suitable for the robotic drive systems as the tracking errors are too high, while the proposed CIFT-tuned cascade controller has better performance, resulting in the reduction of position-tracking error. There are some peaks of tracking errors that are mainly caused by actuator reversal, rotation clearances of and angle gears and

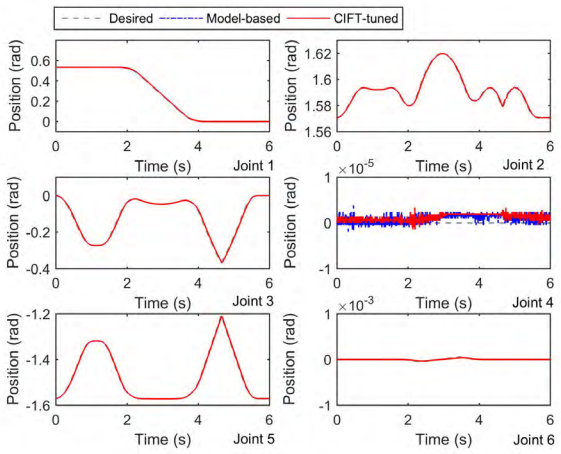

FIGURE 7. Position path-tracking of each joint in case 1.

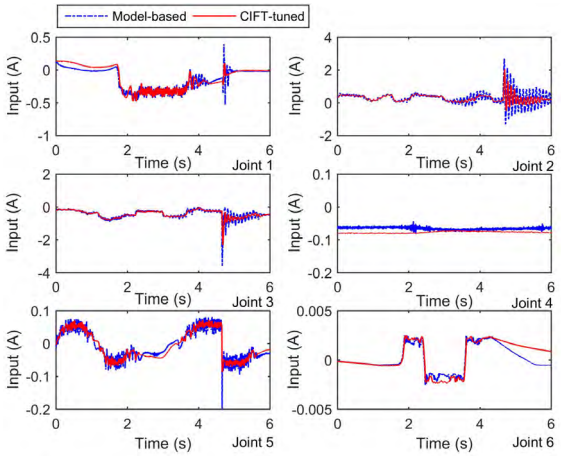

FIGURE 9. Control input of each actuator in case 1.

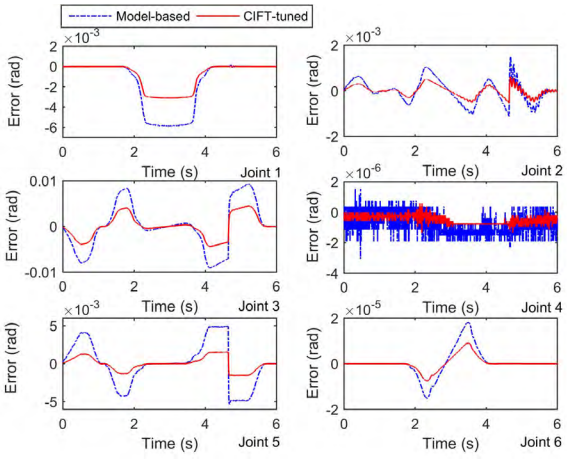

FIGURE 8. Position tracking error of each joint in case 1.

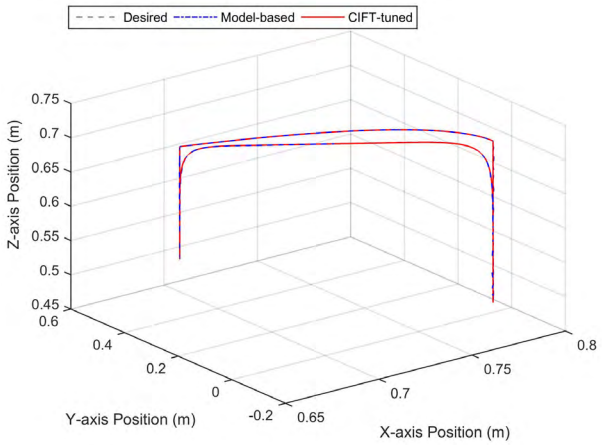

FIGURE 10. Position tracking of the end-effect in case 1.

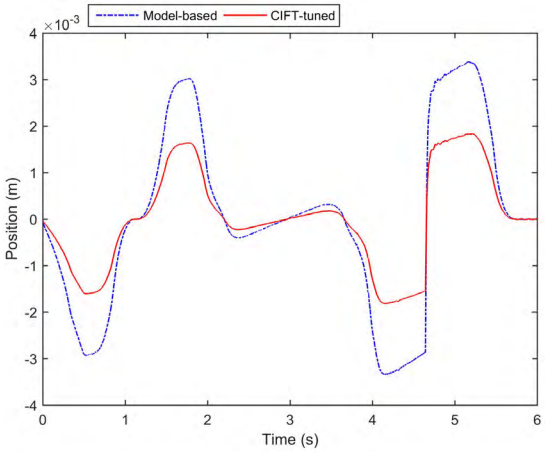

FIGURE 11. Position tracking error of the end-effect in case 1.

coulomb friction, especially when the robot arm changes the directions.

It is noted that the CITF-tuned cascade controller has the capacity of providing better robustness against these external disturbances among the comparison controllers. Take joint 5 for example, the maximum position error for model-based cascade controller and CIFT-tuned controller are 5.3×10^{-3}rad, 1.5×10^{-3}rad, respectively. Hence, the dynamic following performance of the resulting system is improved via the proposed method. Fig. 9 shows the control input currents of robotic joints, and we can see smoother control input signal using the proposed method with decreased magnitude. Some high peak inputs caused by gravity and undesired disturbances are eliminated, especially for joints 1, 3 and 5. A subdued control input signal leads to smaller overshoot and position vibration.

For the end-effect path-tracking, Fig. 10 and Fig. 11 presents the position responses and the corresponding tracking errors, respectively. Comparing to the traditional model-based method, the resulting system using the model-free CIFT-tuned cascade method behaves closely as the desired reference free from the influences of the system uncertainties and unmodeled dynamics. To be more specific, the maximum path-tracking error of the end-effect is decreased by 54.6827%.

TABLE 3. Tracking performance indexes of the joints in Case 1.

Joint	Methods	Indexes (10^{-4})			
		Max	SD	RME	ITAE
1	Model-based	59.1002	24.0207	28.7826	95.1601
	CIFT-tuned	31.0519	9.7370	12.2647	40.4873
2	Model-based	14.9383	3.1210	4.9844	23.3190
	CIFT-tuned	5.26768	1.3174	1.9839	9.2730
3	Model-based	92.7499	34.3237	51.1057	227.1990
	CIFT-tuned	40.2518	13.6474	20.7678	99.0040
4	Model-based	0.0306	0.0052	0.0097	0.0494
	CIFT-tuned	0.0134	0.0025	0.0055	0.0298
5	Model-based	53.4937	19.3370	28.6216	126.6188
	CIFT-tuned	15.9814	6.0212	8.8708	39.0883
6	Model-based	0.1806	0.0500	0.0583	0.1793
	CIFT-tuned	0.0902	0.0251	0.0292	0.0901

TABLE 4. Performance indexes of the end-effect in Case 1.

Methods	Indexes (10^{-4})			
	Max	SD	RME	ITAE
Model-based	33.9310	12.8236	19.0928	84.8733
CIFT-tuned	15.3766	6.9612	9.3693	33.1151

To show the comparison results more clearly, Table 3 and Table 4 present the quantitative performance indexes of the actuated joints and end-effect, separately. According to Table 3 and Table 4, the proposed method outperforms the traditional method with respect to maximum, standard derivation (SD), root mean error (RME) and integrated time absolute error (ITAE). The experimental results verify the effectiveness and control superiority of the proposed CIFT-tuned cascade controller, which can achieve better dynamic path-tracking performance with higher accuracy. By employing the proposed cascade control method, the dynamic tracking errors are reduced up to 1/2 than that using the model-based method.

2) *Case 2:* To verify the robustness of the proposed cascade controller against the external disturbances and systematic uncertainties, the experiment is performed when the payload is attached to the end-effect.

TABLE 5. The tuned parameters using CIFT method in Case 2.

Parameters	Joint					
	1	2	3	4	5	6
K_p	1.24	1.51	1.36	0.79	1.58	0.83
K_s	4.32	3.87	4.06	2.78	4.43	2.82
K_I	0.0284	0.0293	0.0358	0.0204	0.0542	0.0208

For this case, the position trajectory keeps the same with case 1 under a period of 6 s. The final tuned cascade control parameters are shown in Table 5. Fig. 12 and Fig. 13 show the position profile and the tracking error between the feedback and the desired one, respectively. It should be mentioned that coupling, pose position and orientation of the six-DOF structure contribute to time-varying dynamics affecting the

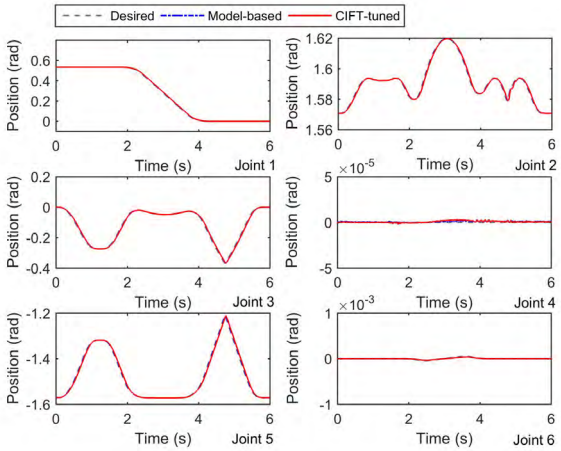

FIGURE 12. Position path-tracking of each joint in case 2.

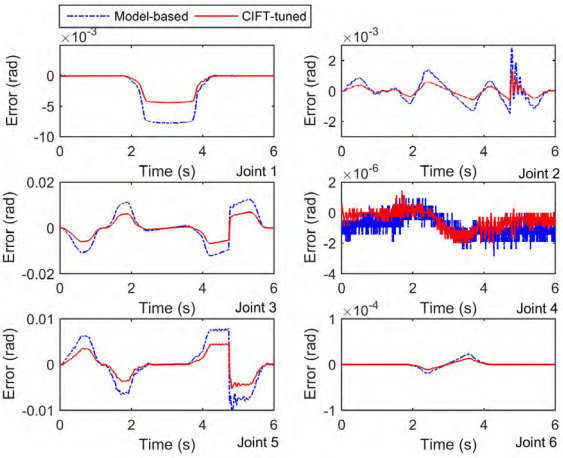

FIGURE 13. Position tracking error of each joint in case 2.

path-tracking performance of the robotic system. The experimental test demonstrates that, by using the proposed method, the path-tracking performance of each joint is enhanced observably, especially for joints 2 and 5, where the system dynamics change rapidly due to the pose position and the additional payload.

As given in Table 6, we have provided the performances of the joints in terms of the maximum value, SD, RME and the traditional ITAE, which verifies that the CIFT-tuned cascade controller can obtain better performance indexes. Take joint 5 for example, the ITAEs of the proposed controller and the traditional controller is 194.0921 rad and 57.2985 rad, separately. From the experimental results of Fig. 9 and Fig 14, it is known that larger control inputs are needed to drive each joint to limit the impact of the payload so that the end-effect can achieve the desired position. Moreover, compared with the model-based tuned cascade controller, the current vibration of the joints has been significantly improved, resulting in smoother position trajectories for all the actuated joints.

With regards to the final end-effect position-tracking, compared to the conventional model-based tuning method, the

TABLE 6. Tracking performance indexes of the joints in Case 2.

Joint	Methods	Indexes (10^{-4})			
		Max	SD	RME	ITAE
1	Model-based	77.9789	31.8212	38.1702	126.5048
	CIFT-tuned	39.8865	11.9198	14.2893	56.1761
2	Model-based	28.3856	4.3328	6.8395	31.7438
	CIFT-tuned	9.5292	1.8928	2.2827	11.8202
3	Model-based	124.6084	46.1314	69.0155	308.0166
	CIFT-tuned	48.4911	18.7239	28.3144	120.3575
4	Model-based	0.0287	0.0536	0.0104	0.0536
	CIFT-tuned	0.0201	0.0052	0.0075	0.0212
5	Model-based	98.4527	30.0116	44.1926	194.0912
	CIFT-tuned	46.6810	9.1658	12.7875	57.2985
6	Model-based	0.2271	0.0626	0.0703	0.2249
	CIFT-tuned	0.1357	0.0375	0.0437	0.1347

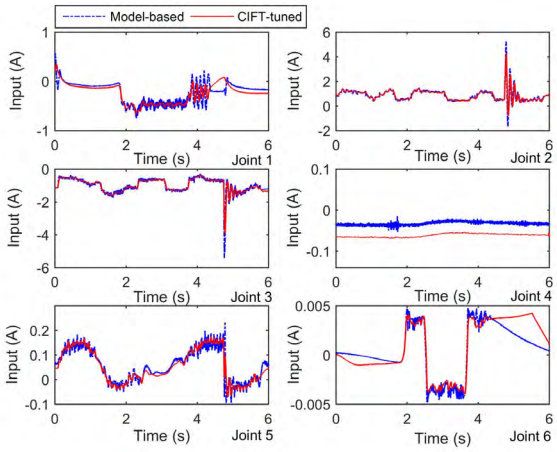

FIGURE 14. Control input of each joint in case 2.

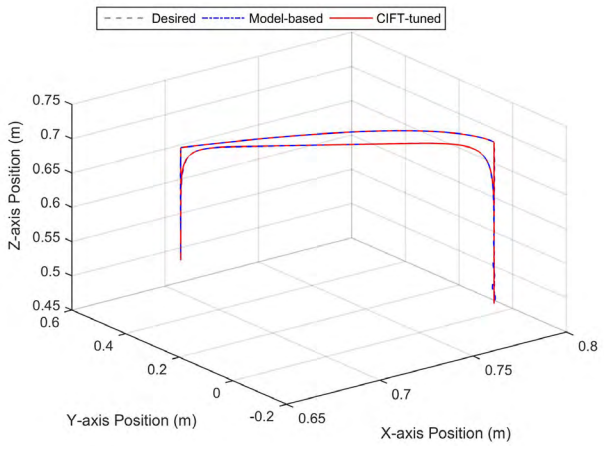

FIGURE 15. Position tracking of the end-effect in case 2.

proposed CIFT-tuned cascade controller shows improved path-tracking performance, as depicted in Fig. 15 and Fig. 16. Comparing Fig. 16 (Case 2) and Fig. 11 (Case 1), the system path-tracking errors of the joints are increased when attaching the additional payload to the end-effect. Superior to the traditional model-based method, the resulting system can maintain

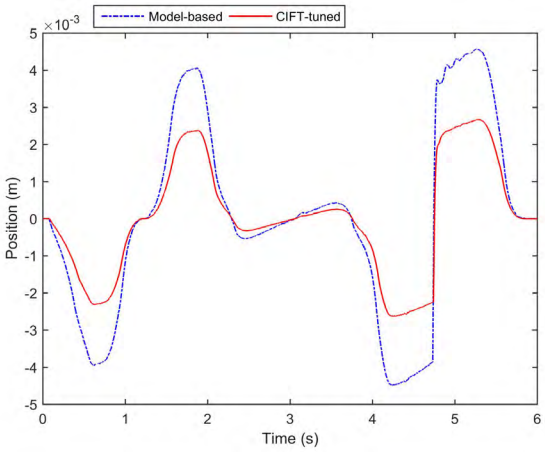

FIGURE 16. Position tracking error of the end-effect in case 2.

TABLE 7. Performance indexes of the end-effect in Case 2.

Methods	Indexes (10^{-4})			
	Max	SD	RMS	ITAE
Model-based	44.7983	17.2348	25.7750	115.4728
CIFT-tuned	21.7210	9.1864	13.0391	53.9374

superior dynamics under the control of the proposed method. The quantitative performance indexes are provided in Table 7. From the test, it is shown that the maximum value, SD, RMS and ITAE can reach up to 51.5137%, 46.6985%, 49.4118% and 53.2899%, respectively. Therefore, we can conclude that our method guarantees the system robustness to against the unknown disturbances, including lumped parametric uncertainties, unmodeled dynamics and torque fluctuation.

V. CONCLUSIONS

In this paper, a CIFT-tuned cascade controller had been developed to achieve a robust path-tracking of a developed networked industrial robot. The proposed CIFT-tuned method is a data-based model-free method without explicit mathematical model information of the robotic system to be controlled. By incorporating the tracking error and control input magnitude into the objective criterion, a multi-DOF CIFT method was constructed to give an optimal design of the cascade control parameters. Theoretical analysis illustrated that the unbiased estimate of the gradient and the asymptotic accuracy can be guaranteed. Two comparative experiments were performed to verify the effectiveness of the proposed method, and the results indicated that this newly developed method possesses control advantages in terms of robust path-tracking against the parametric uncertainties and external disturbances. It was also demonstrated that the resulting industrial robotic system has an adaptive learning ability to accommodate different operating situations. Thus, the practical CIFT cascade control method is potential for the networked industrial robots

because of its model-free features, satisfactory tracking performance, robust nature and simplicity for implementation.

Additionally, future work will be directed toward the compensation techniques for data disturbances and intermittent transmission to improve the position path-tracking performance of the industrial robot. In this paper, the network communication protocol ensures a stable data-transmission between the robotic upper controller and the remote servo drive control systems. Nevertheless, the control performance of the resulting systems will be affected by measurement noise and missing packages when the proposed method is applied to a highly noisy application, which is considered and eliminated in our ongoing research.

REFERENCES

[1] S. Robla-Gómez, V. M. Becerra, J. R. Llata, E. González-Sarabia, C. Torre-Ferrero, and J. Pérez-Oria, "Working together: A review on safe human-robot collaboration in industrial environments," *IEEE Access*, vol. 5, pp. 26754–26773, 2017.

[2] E. A. Padilla-Garcia, A. Rodriguez-Angeles, J. R. Reséndiz, and C. A. Cruz-Villar, "Concurrent optimization for selection and control of AC servomotors on the powertrain of industrial robots," *IEEE Access*, vol. 6, pp. 27923–27938, 2018.

[3] I. Bonilla, M. Mendoza, E. J. Gonzalez-Galván, C. Chavez-Olivares, A. Loredo-Flores, and F. Reyes, "Path-tracking maneuvers with industrial robot manipulators using uncalibrated vision and impedance control," *IEEE Trans. Syst., Man, Cybern. C, Appl. Rev.*, vol. 42, no. 6, pp. 1716–1729, Nov. 2012.

[4] T. Faulwasser, T. Weber, P. Zometa, and R. Findeisen, "Implementation of nonlinear model predictive path-following control for an industrial robot," *IEEE Trans. Control Syst. Technol.*, vol. 25, no. 4, pp. 1505–1511, Jul. 2017.

[5] Y. M. Zhao, Y. Lin, F. Xi, and S. Guo, "Calibration-based iterative learning control for path tracking of industrial robots," *IEEE Trans. Ind. Electron.*, vol. 62, no. 5, pp. 2921–2929, May 2015.

[6] J. Lee, P. H. Chang, and M. Jin, "Adaptive integral sliding mode control with time-delay estimation for robot manipulators," *IEEE Trans. Ind. Electron.*, vol. 64, no. 8, pp. 6796–6804, Aug. 2017.

[7] X. Yin and L. Pan, "Enhancing trajectory tracking accuracy for industrial robot with robust adaptive control," *Robot. Comput.-Integr. Manuf.*, vol. 51, pp. 97–102, Jun. 2018.

[8] H. C. Cho, M. S. Fadali, K. S. Lee, and N. H. Kim, "Adaptive position and trajectory control of autonomous mobile robot systems with random friction," *IET Control Theory Appl.*, vol. 4, no. 12, pp. 2733–2742, 2010.

[9] Y. I. Son, I. H. Kim, D. S. Choi, and H. Shim, "Robust cascade control of electric motor drives using dual reduced-order PI observer," *IEEE Trans. Ind. Electron.*, vol. 62, no. 6, pp. 3672–3682, Jun. 2015.

[10] S. Kissling, P. Blanc, P. Myszkorowski, and I. Vaclavik, "Application of iterative feedback tuning (IFT) to speed and position control of a servo drive," *Control Eng. Pract.*, vol. 17, no. 7, pp. 834–840, 2009.

[11] Z. Du, D. Yue, and S. Hu, "H-infinity stabilization for singular networked cascade control systems with state delay and disturbance," *IEEE Trans. Ind. Informat.*, vol. 10, no. 2, pp. 882–894, May 2014.

[12] H. Guo, Y. Liu, G. Liu, and H. Li, "Cascade control of a hydraulically driven 6-DOF parallel robot manipulator based on a sliding mode," *Control Eng. Pract.*, vol. 16, no. 9, pp. 1055–1068, 2008.

[13] N. Nedic, D. Prsic, L. Dubonjic, V. Stojanovic, and V. Djordjevic, "Optimal cascade hydraulic control for a parallel robot platform by PSO," *Int. J. Adv. Manuf. Technol.*, vol. 72, nos. 5–8, pp. 1085–1098, 2014.

[14] Y. Pi and X. Wang, "Observer-based cascade control of a 6-DOF parallel hydraulic manipulator in joint space coordinate," *Mechatronics*, vol. 20, no. 6, pp. 648–655, 2010.

[15] X. Zhao, P. Shi, and X. Zheng, "Fuzzy adaptive control design and discretization for a class of nonlinear uncertain systems," *IEEE Trans. Cybern.*, vol. 46, no. 6, pp. 1476–1483, Jun. 2016.

[16] X. Zhao, X. Wang, G. Zong, and H. Li, "Fuzzy-approximation-based adaptive output-feedback control for uncertain nonsmooth nonlinear systems," *IEEE Trans. Fuzzy Syst.*, vol. 26, no. 6, pp. 3847–3859, Dec. 2018.

[17] K. A. Saar, F. Giardina, and F. Iida, "Model-free design optimization of a hopping robot and its comparison with a human designer," *IEEE Robot. Autom. Lett.*, vol. 3, no. 2, pp. 1245–1251, Apr. 2018.

[18] M. Li, R. Kang, D. T. Branson, and J. S. Dai, "Model-free control for continuum robots based on an adaptive Kalman filter," *IEEE/ASME Trans. Mechatronics*, vol. 23, no. 1, pp. 286–297, Feb. 2018.

[19] Y. Xie, X. Tang, S. Zheng, W. Qiao, and B. Song, "Adaptive fractional order PI controller design for a flexible swing arm system via enhanced virtual reference feedback tuning," *Asian J. Control*, vol. 20, no. 3, pp. 1221–1240, 2018.

[20] W. Zheng, Y. Luo, Y. Chen, and Y. Pi, "Fractional-order modeling of permanent magnet synchronous motor speed servo system," *J. Vib. Control*, vol. 22, no. 9, pp. 61–66, 2015.

[21] A. T. Azar and F. E. Serrano, "Robust IMC–PID tuning for cascade control systems with gain and phase margin specifications," *Neural Comput. Appl.*, vol. 25, no. 5, pp. 983–995, 2014.

[22] M. Li, Y. Zhu, K. Yang, L. Yang, C. Hu, and H. Mu, "Convergence rate oriented iterative feedback tuning with application to an ultraprecision wafer stage," *IEEE Trans. Ind. Electron.*, vol. 66, no. 3, pp. 1993–2003, Mar. 2019.

[23] K. Hamamoto, T. Fukuda, and T. Sugie, "Iterative feedback tuning of controllers for a two-mass-spring system with friction," *Control Eng. Pract.*, vol. 11, no. 9, pp. 1061–1068, 2003.

[24] W. Meng, S. Q. Xie, Q. Liu, C. Z. Lu, and Q. Ai, "Robust iterative feedback tuning control of a compliant rehabilitation robot for repetitive ankle training," *IEEE/ASME Trans. Mechatronics*, vol. 22, no. 1, pp. 173–184, Feb. 2017.

[25] R. Chi, Z. Hou, S. Jin, D. Wang, and J. Hao, "A data-driven iterative feedback tuning approach of ALINEA for freeway traffic ramp metering with PARAMICS simulations," *IEEE Trans Ind. Informat.*, vol. 9, no. 4, pp. 2310–2317, Nov. 2013.

[26] M. F. Heertjes, B. Van der Velden, and T. Oomen, "Constrained iterative feedback tuning for robust control of a wafer stage system," *IEEE Trans. Control Syst. Technol.*, vol. 24, no. 1, pp. 56–66, Jan. 2016.

[27] D. A. Tesch, D. Eckhard, and W. C. Guarienti, "Pitch and roll control of a quadcopter using cascade iterative feedback tuning," *IFAC-PapersOnLine*, vol. 49, no. 30, pp. 30–35, 2016.

[28] D. Tesch, D. Eckhard, and A. S. Bazanella, "Iterative feedback tuning for cascade systems," in *Proc. IEEE Eur. Control Conf. (ECC)*, Aalborg, Denmark, Jun./Jul. 2016, pp. 495–500.

[29] X.-H. Chang, J. Xiong, Z.-M. Li, and J. H. Park, "Quantized static output feedback control for discrete-time systems," *IEEE Trans. Ind. Informat.*, vol. 14, no. 8, pp. 3426–3435, Aug. 2018.

[30] X.-H. Chang, Z.-M. Li, and J. H. Park, "Fuzzy generalized $\mathcal{H}_2$ filtering for nonlinear discrete-time systems with measurement quantization," *IEEE Trans. Syst., Man, Cybern., Syst.*, vol. 48, no. 12, pp. 2419–2430, Dec. 2018.

[31] Y. Xie, X. Tang, B. Song, X. Zhou, and Y. Guo, "Data-driven adaptive fractional order PI control for PMSM servo system with measurement noise and data dropouts," *ISA Trans.*, vol. 75, pp. 172–188, Apr. 2018.

[32] W. He, Y. Dong, and C. Sun, "Adaptive neural impedance control of a robotic manipulator with input saturation," *IEEE Trans. Syst., Man, Cybern., Syst.*, vol. 46, no. 3, pp. 334–344, 2016.

[33] M. Mendoza, A. Zavala-Río, V. Santibáñez, and F. Reyes, "Output-feedback proportional–integral–derivative-type control with simple tuning for the global regulation of robot manipulators with input constraints," *IET Control Theory Appl.*, vol. 9, no. 14, pp. 2097–2106, 2015.

[34] X. Chen, Y. Jia, and F. Matsuno, "Tracking control for differential-drive mobile robots with diamond-shaped input constraints," *IEEE Trans. Control Syst. Technol.*, vol. 22, no. 5, pp. 1999–2006, Sep. 2014.

[35] X.-H. Chang and Y.-M. Wang, "Peak-to-peak filtering for networked nonlinear dc motor systems with quantization," *IEEE Trans. Ind. Informat.*, vol. 14, no. 12, pp. 5378–5388, Dec. 2018.

[36] X. Chen and Y. Jia, "Input-constrained formation control of differential-drive mobile robots: Geometric analysis and optimisation," *IET Control Theory Appl.*, vol. 8, no. 7, pp. 522–533, 2014.

[37] S.-R. Oh and S. K. Agrawal, "The feasible workspace analysis of a set point control for a cable-suspended robot with input constraints and disturbances," *IEEE Trans. Control Syst. Technol.*, vol. 14, no. 4, pp. 735–742, Jul. 2006.

[38] J. K. Huusom, N. K. Poulsen, and S. B. Jørgensen, "Improving convergence of iterative feedback tuning," *J. Process Control*, vol. 19, no. 4, pp. 570–578, Apr. 2009.

[39] H. Wang, B. Chen, X. Liu, K. Liu, and C. Lin, "Robust adaptive fuzzy tracking control for pure-feedback stochastic nonlinear systems with input constraints," *IEEE Trans. Cybern.*, vol. 43, no. 6, pp. 2093–2104, Dec. 2013.
[40] R. Hildebrand, A. Lecchini, G. Solari, and M. Gevers, "Optimal prefiltering in iterative feedback tuning," *IEEE Trans. Autom. Control*, vol. 50, no. 8, pp. 1196–1200, Aug. 2005.
[41] R. Hildebrand, A. Lecchini, G. Solari, and M. Gevers, "Prefiltering in iterative feedback tuning: Optimization of the prefilter for accuracy," *IEEE Trans. Autom. Control*, vol. 49, no. 10, pp. 1801–1806, Oct. 2004.

YUANLONG XIE received the B.S. degree in electrical engineering and the Ph.D. degree in mechanical engineering from the Huazhong University of Science and Technology (HUST), Wuhan, China, in 2014 and 2018, respectively.

He was an Academic Visitor with the School of Electronic and Electrical Engineering, University of Leeds, Leeds, U.K., from 2017 to 2018. He has been a Postdoctoral Fellow with HUST, since 2018.

He has published more than 15 academic journal and conference papers, and holds six patents. His research interests include servo control, field-bus technology, and networked control systems.

JIAN JIN received the master's degree in mechanical automation from the Huazhong University of Science and Technology (HUST), Wuhan, China, in 1989.

She is currently an Associate Professor with the School of Mechanical Science and Engineering, HUST. Her current research interests include the reliability of industrial automation technology and numerical control system.

XIAOQI TANG received the Ph.D. degree in mechanical engineering from the Huazhong University of Science and Technology (HUST), Wuhan, China, in 1998.

He was an Academic Visitor with the School of Engineering, The Hong Kong University of Science and Technology, Hong Kong, from 1996 to 1998. He is currently a Professor with HUST, where he is also the Vice Director of the National NC System Engineering Research Center.

He has co-authored three books, has published more than 100 international conference and journal papers, and holds more than 30 patents. His research interests include servo control and intelligent machinery manufacturing.

BOSHENG YE received the M.S. and Ph.D. degrees from Northwestern Polytechnical University, Xi'an, China, in 1991 and 1994, respectively.

From 1994 to 1997, he was a Postdoctoral Fellow with the Huazhong University of Science and Technology, where he is currently an Associate Professor. His current research interests include robot control, CNC technology, and intelligent manufacturing.

JIEYU TAO received the B.S. degree from Chongqing University, Chongqing, China, in 2016. She is currently pursuing the M.S. degree in mechanical engineering with the Huazhong University of Science and Technology. Her current research interests include system identifications and robot control.